THE JOURNAL OF PHYSICAL CHEMISTRY B

Article

pubs.acs.org/JPCB

Computed and Experimental Chemical Shift Parameters for Rigid and Flexible YAF Peptides in the Solid State

Tomasz Pawlak,[†] Katarzyna Trzeciak-Karlikowska,[†] Jiri Czernek,[‡] Wlodzimierz Ciesielski,[†] and Marek J. Potrzebowski*[,†]

[†]Centre of Molecular and Macromolecular Studies, Polish Academy of Sciences, Sienkiewicza 112, PL-90-363 Lodz, Poland

[‡]Institute of Macromolecular Chemistry, Academy of Sciences of the Czech Republic, Heyrovsky Square 2, CZ-16206 Praha 6, Czech Republic

Supporting Information

ABSTRACT: DFT methods were employed to compute the ^{13}C NMR chemical shift tensor (CST) parameters for crystals of YAF peptides (Tyr-Ala-Phe) with different stereochemistry for the Ala residue. Tyr-D-Ala-Phe **1** crystallizes in the *C*2 space group while Tyr- L-Ala-Phe crystallizes in either the $P2_12_12$ space group (**2a**) or the $P6_5$ space group (**2b**). PISEMA MAS measurements for samples with a natural abundance of ^{1}H and ^{13}C nuclei and ^{2}H QUADECHO experiments for samples with deuterium labeled aromatic rings were used to analyze the geometry and time scale of the molecular motion. At ambient temperature, the tyrosine ring of sample **1** is rigid and the phenylalanine ring undergoes a π-jump, both rings in sample **2a** are static, and both rings in sample **2b** undergo a fast regime exchange. The theoretical values of the CST were obtained for isolated molecules (IM) and clusters employing the ONIOM approach. The experimental ^{13}C δ_{ii} parameters for all of the samples were measured via a 2D PASS sequence. Significant scatter of the computed versus the experimental ^{13}C CST parameters was observed for **1** and **2b,** while the observed correlation was very good for **2a**. In this report, we show that the quality of the ^{13}C σ_{ii}/^{13}C δ_{ii} correlations, when properly interpreted, can be a source of important information about local molecular motions.

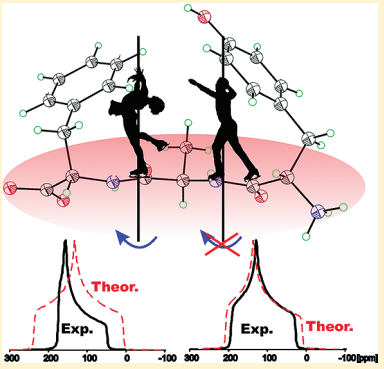

INTRODUCTION

The nuclear magnetic resonance (NMR) chemical shift (CS) is one of the most important structural parameters that can be obtained from the spectroscopic methods.[1,2] The CS is very useful in structure analysis, because it provides insight into the underlying mechanism of nuclear shielding including the dependence on molecular conformational changes and intra-(inter)molecular interactions, such as hydrogen bonding and aromatic−aromatic interactions as well as the ionization state.[3] The power of NMR spectroscopy is due to the ability to use this technique with all kinds of materials including gases, liquids, solids, and semisolids. For gas and solution-state NMR, the assignment of chemical shifts to molecular structures can be performed by employing one-dimensional and/or two-dimensional experiments, examination of empirical tables of chemical shifts or application of quantum mechanics (QM) methods, which are currently used to calculate the CS for nuclei in a variety of molecules.[4,5] At the beginning of development QM methods, the methods based on semiempirical, ab inito or DFT (density functional theory) approaches have remained qualitative in their prediction of experimental data.[6,7] With recent progress in quantum mechanics calculations, the accuracy of computed nuclear shielding parameters for gases and liquids with respect to experimental data is excellent in many cases.[8] For the solid matter, the assignment of CS parameters is more complex, because the number of so-called "solid state effects", such as intermolecular contacts, molecular disorder, presence of polymorphs, etc., play a significant role.[9] Another factor that can greatly complicate calculation of the chemical shift parameters is the molecular dynamics in the solid state. Recently, this problem was exhaustively discussed by several authors.[10] Dumez and Pickard, who employed well-defined crystalline organic solids, have tested the influence of molecular motion on the quality of theoretical data using density functional theory calculations performed within the plane-wave pseudopotential framework.[11] In the cited work, the influence of motional effects was assessed by averaging over the vibrational modes or over snapshots taken from ab initio molecular dynamics simulations. A similar approach was recently applied by Vendruscolo and co-workers, who showed that molecular motion has a great influence on the accuracy of chemical shift calculations when using the gauge including projector augmented wave (GIPAW) method, which accounts for the periodic nature of the crystal structure.[12] This effect was discussed for *N*-formyl-L-methionyl-L-leucyl-L-phenylalanine-OMe (MLF), which is a relatively rigid peptide system that has been very well characterized experimentally by XRD and has been used to develop of number of solid-state NMR

Received: November 19, 2011
Revised: January 12, 2012
Published: January 12, 2012

techniques. The role of small-amplitude motion, its influence on ^{13}C chemical shielding tensors and quality of DFT calculations was recently reported by Geppi and co-workers.[13]

The challenge for modern QM methodology is the correlation of experimental and theoretical NMR chemical shift parameters for solid-state systems with large amplitude molecular motions. For several reasons, peptides appear to be good candidates for such projects. It is well-known that peptides are relatively small biological entities (compared to proteins or nucleic acids). In physiological environments, they are flexible molecules with molecular flexibility encoded in their primary structure. Flexibility is required to perform their natural biological functions and to control processes, such as molecular recognition, ligand binding and catalysis.

In this work, we present a detailed analysis of the structure and molecular dynamics in the crystal lattice of YAF (Tyr-Ala-Phe) peptides with varying alanine residue stereochemistry (L and D) and comparison of experimentally measured chemical shift parameters with computed NMR data. Such models can be further used for developing of more advanced QM methodologies implementing large amplitude motions.

Tyr-D-Ala-Phe (Scheme 1) is a message sequence of deltorphin I (Tyr-D-Ala-Phe-Asp-Val-Val-Gly-NH_2), deltorphin

Scheme 1. Molecular Structure and Numbering System of YAF

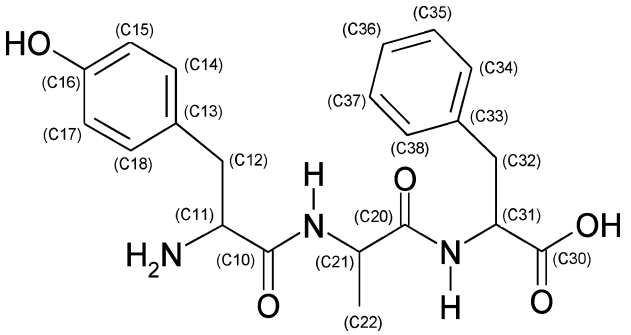

II (Tyr-D-Ala-Phe-Glu-Val-Val-Gly-NH_2), and dermorphin (Tyr-D-Ala-Phe-Gly-Tyr-Pro-Ser-NH_2), which are opioid peptides extracted from the skin of South American frogs.[14] The presence of D-amino acid is crucial for biological activity. It is interesting to note that heptapeptides consisting of L-alanine are not analgesics.[15] Analysis of the influence of stereochemistry on molecular packing, dynamics and biological functions of neuropeptides is still challenging not only for theoretical chemistry (e.g., QM calculations) but also for practical applications (e.g., design of new selective pain killers).

EXPERIMENTAL SECTION

NMR. The solid-state magic angle spinning (MAS) experiments were performed on a BRUKER Avance III 400 spectrometer at a frequency of 100.613 MHz for ^{13}C equipped with a MAS probe head using 4 mm ZrO_2 rotors. A sample of glycine was used to set the Hartmann–Hahn condition, and glycine was used as a secondary chemical shift reference δ = 176.04 ppm from the external TMS.[16] The conventional spectra were recorded with a proton 90° pulse length of 4 μs and a contact time of 2 ms. The repetition delay was 6 s, and the spectra width was 25 kHz. The FIDs were accumulated using a time domain size of 2 K data points. The RAMP shape pulse[17] was used during the cross-polarization and TPPM decoupling.[18] The spectral data were processed using the TOPSPIN program.[19] The 61.42 MHz ^2H NMR spectra were recorded employing a quadrupole echo pulse sequence without sample spinning and a 90° pulse length of 3 μs.

For the PISEMA MAS experiment,[20] the ^1H effective field strength was 50 kHz in all of the experiments, and the ^{13}C spin-lock field strengths was adjusted to the first-order sideband condition, $\omega_{13C} = \omega_{1Heff} \pm \omega_r$. The spinning speed was 13 kHz and was regulated to ±3 Hz by a pneumatic control unit. Recycle delays varied from 1.5 to 4 s. The 2D PISEMA MAS experiments incremented the SEMA contact time at a step of 16.28 μs. At a spinning speed of 13 kHz, the dwell time for the evolution period was 19.23 μs. The maximum t_1 evolution time was typically approximately 1 ms. Only cosine-modulated data were collected. Thus, a real Fourier transformation was performed on the t_1 data yielding spectra with a symmetrized ω_1 dimension and showing the dipolar splittings. Because the t_1 time signal increases with increasing SEMA contact time, the ω_1 dimension was processed using the baseline correction mode "qfil" in the TOPSPIN software, which subtracts a constant intensity from the time signals prior to the Fourier transformation yielding spectra free of a dominant zero-frequency peak giving the $^1H-^{13}C$ doublet.

A 5-π pulse 2D PASS scheme and 1000 Hz sample spinning speeds were used in the 2D experiments. The π-pulse length was 8 μs. Sixteen t_1 increments using the timings described by Levitt and co-workers were used in the 2D PASS experiments.[21] For each increment, 360 scans were accumulated. Because the pulse positions in the t_1 set return to their original positions after a full cycle and the t_1-FID forms a full echo, the 16-point experimental t_1 data were replicated to 256 points. After the Fourier transformation in the direct dimension, the 2D spectrum was sheared to align all side bands with the center bands in the indirect dimension of the 2D spectrum. One-dimensional CSA spinning sideband patterns were obtained from t_1 slices taken at the isotropic chemical shifts in the t_2 dimension of the 2D spectrum. The magnitudes of the principal elements of the CSA tensor were obtained from the best-fit simulated spinning sideband pattern. Simulations of the spinning CSA sideband spectra were performed on a PC using the Topspin program.

QM Calculations. The quantum chemical calculations were performed using Gaussian 09.[22] For the calculations, the scf = tight keyword was employed (i.e., convergence to 10^{-8} for the energy and to 10^{-6} for the density matrix). An ultrafine grid with 75 radial shells and 302 angular points has been employed. The calculations were performed without any symmetry restrictions.

DFT Calculations for the Isolated Molecules (IMs) of ***1****,* ***2a****, and* ***2b****.* The starting structures for the geometry optimizations were the X-ray geometries (CCDC codes 222456, 720511 and 720512).[23,24] The B3LYP[25,26] method has been used with the Pople 6-311G** basis set[27−29] for optimization of the proton positions only. All of the calculations were performed for a single in vacuo molecule. The optimized geometries were used to calculate the nuclear magnetic shielding by means of DFT using the gauge including atomic orbitals (GIAO) method.[30] We used the hybrid functional PBE0[31,32] with the 6-311++G** basis set.

DFT Calculations for Clusters of ***1****,* ***2a*** *and* ***2b*** *Employing the ONIOM Approach.*[33] To reduce the computational time, the ONIOM method as programmed in the Gaussian 09 computer program was employed for calculation of the clusters.

dx.doi.org/10.1021/jp2111567 | J. Phys. Chem. B 2012, 116, 1974−1983

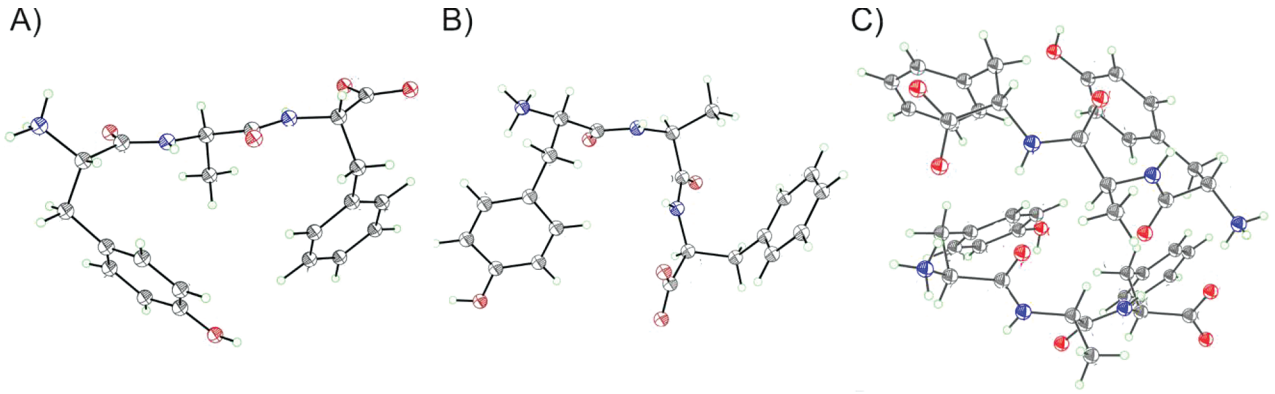

Figure 1. Molecular structures of tripeptide (A) sample **1**, (B) sample **2a**, and (C) sample **2b** with ellipsoids at 50% probability.

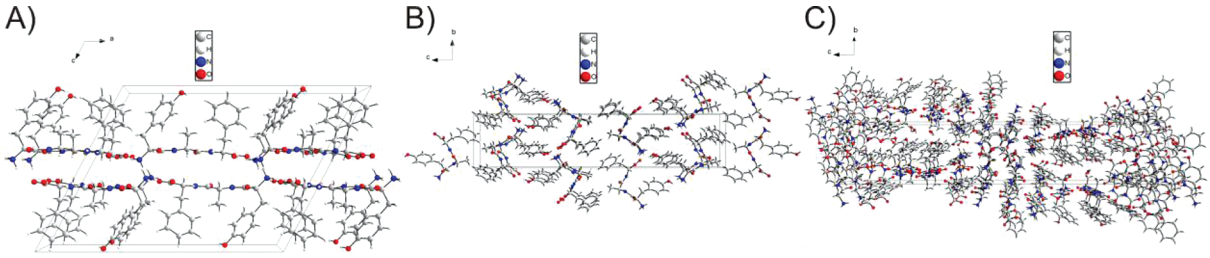

Figure 2. Unit cells containing (A) four molecules of tripeptide **1**, (B) four molecules of tripeptide **2a**, and (C) twelve molecules of tripeptide **2b**.

ONIOM divides the system into three segments, which can be treated at different levels of calculational complexity. Therefore, one can treat the critical part of the system at a high level, while the less critical parts of the system might be calculated at a medium or low level. For this study, we used two ONIOM levels (i.e., high and low). The part of the system treated with the high level included molecules from the independent part of the unit cell (one molecule of YAF for the **1** and **2a** structures and two molecules of YAF for the **2b** structure). The part of system treated with the low level included molecules of the YAF peptide that exhibit short contacts to atoms from the high-level part of the system (short contacts observed in the X-ray structures). The clusters employed for the calculations are presented in the Supporting Information. For optimization of the proton coordinates we used a two layer ONIOM with the DFT hybrid functional B3LYP and the 6-311G** basis set for the high layer and a molecular mechanics methods with an universal force field (UFF).[34] For the GIAO NMR calculations of all of the cases, we used the B3LYP functional and the 6-311++G** basis sets as the high layer and UFF molecular modeling as the low layer.

NMR Chemical Shifts. The choice of the reference compound can partially eliminate systematic errors in the DFT calculations of the chemical shifts.[35] In this study, one reference compound could not be selected for all molecular structures. Therefore, we have calculated the chemical shifts using the equation $\delta_i = \Delta_{SF} - \sigma_i$ where Δ_{SF} is the scaling factor determined from correlation between the experimental δ_{iso} and the theoretical σ_{iso} parameter and minimization of the rmsd value. The same Δ_{SF} value was used to recalculate σ_{ii} onto δ_{ii} parameters. Linearization was performed separately for each of the three molecules in this study.

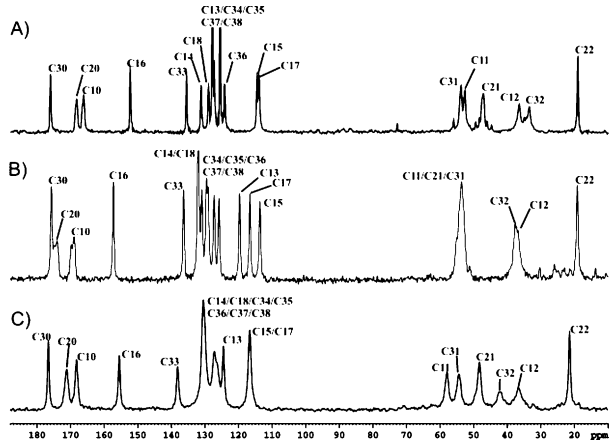

Figure 3. ^{13}C CP/MAS spectra of (A) **1**, (B) **2a**, and (C) **2b** structures.

RESULTS AND DISCUSSION

(i). Assignment of Isotropic Chemical Shifts to Molecular Structure of 1, 2a and 2b by Means of GIAO DFT Calculations. The X-ray data for Tyr-D-Ala-Phe (**1**) and two forms of Tyr-L-Ala-Phe (**2a** and **2b**) have been previously reported.[23,24] Figure 1 shows the molecular structure of the peptides; the unit cells are displayed in Figure 2.

For sample **1**, the crystal system is monoclinic with a space group of *C*2. The unit cell contains four molecules with lattice parameters of a = 23.091(5) Å, b = 5.4940(10) Å, and c = 17.510(4) Å.

Sample **2a** crystallizes in the orthorhombic system with $P2_12_12$ space group. The unit cell contains four molecules, and its lattice parameters are as follow; a = 8.653(2) Å, b = 5.5238 (1) Å, and c = 39.737(8) Å. Sample **2b** crystallizes in the hexagonal system with $P6_5$ space group. The unit cell contains

dx.doi.org/10.1021/jp2111567 | J. Phys. Chem. B 2012, 116, 1974–1983

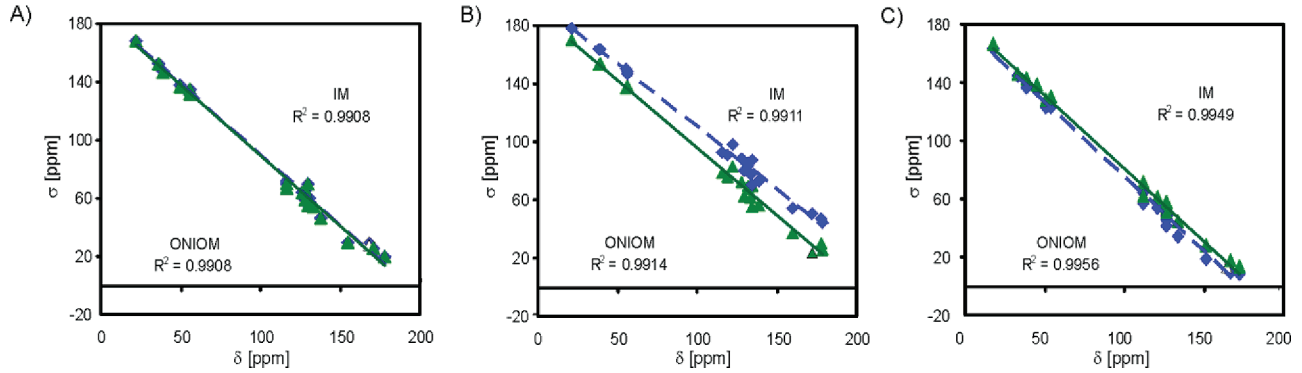

Figure 4. Correlation of the experimental isotropic chemical shift values (δ) as a function of the calculated isotropic nuclear shielding (σ) using IM (blue) and ONIOM (green) data for (A) sample **1**, (B) sample **2a**, and (C) sample **2b**.

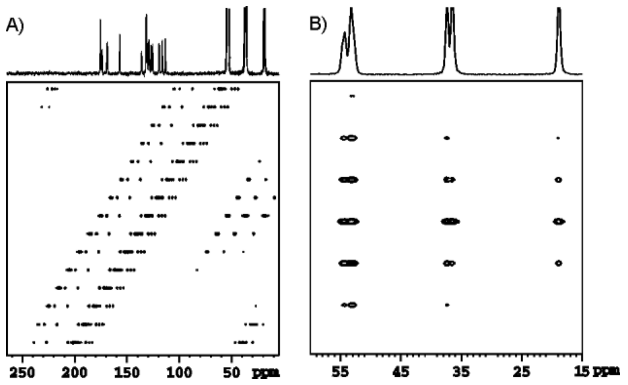

Figure 5. 2D PASS spectra for **2a** recorded with a spinning rate of 1000 Hz (A) and the aliphatic part of spectrum after data shearing (B).

twelve molecules, and its size is much larger compared to **2a**; a = 11.946(2) Å, b = 11.946(2) Å, and c = 54.991(11) Å.

The ^{13}C CP/MAS spectra of **1**, **2a**, and **2b** recorded with a spinning rate of 8 kHz at ambient temperature are shown in Figure 3. It is worthy to note that for sample **2b** two crystalographically nonequivalent molecules in the asymmetric unit of the crystal structure are magnetically equivalent. Due to this effect and molecular dynamics for **2b** we observed spectra as in case of samples with one molecule in the asymmetric unit. The assignment of the ^{13}C isotropic signals was performed via theoretical calculations. Many methods are currently available for computing NMR parameters. In most of the commonly used approaches, GIAO (gauge-including atomic orbitals) with DFT (density functional theory) hybrid functionals are employed.[36] In the absence of dynamical disorder, this strategy can be expected to predict the tensor components within ten ppm from their experimental counterparts.[37] Since ab initio and DFT calculations for large complexes are still very time-consuming, the proper choice of the method and the basis set is crucial to maintaining a balance between the quality of results and the cost.

In the current project, in order to have a full set of data for the **1**, **2a**, and **2b** samples we performed DFT GIAO computations for isolated molecules (IMs) and appropriate clusters (ONIOM approach) employing our previously reported strategy.[38] The calculated NMR shielding parameters are attached as supporting data.

Figure 4 shows plots of the isotropic values of the ^{13}C chemical shifts as a function of the computed shielding parameters. From inspection of the data, a good correlation between the experimental and calculated data is observed. By comparing the slope and fitting quality (R^2) of the correlation functions, it may be concluded that both methods yielded acceptable results. For sample **1** and **2b**, the intercepts for the clusters (ONIOM approach) are comparable, while for **2a**, the intercept was lower compared to the IM calculations. For ONIOM, their values are in the range of 184.8−187.4 ppm. For the IM approach, the intercepts are in the range of 185.6−204.1 ppm. In particular, this value is overestimated for sample **2a** (Figure 4b).

Table 1. Experimental ^{13}C Aliphatic NMR Chemical Shift Tensor Parameters [in ppm] for the Molecular Crystals of 1, 2a, and 2b[a]

structure	atom	δ_{iso}	δ_{11}	δ_{22}	δ_{33}	Ω^b	κ^c
1	C-11	54.1	69	55	38	31	0.09
	C-12	37.8	53	39	21	32	0.11
	C-21	48.2	69	47	29	40	−0.09
	C-22	20.3	41	14	6	35	−0.54
	C-31	54.1	69	55	38	31	0.09
	C-32	34.8	47	38	19	28	0.34
2a	C-11	53.4	71	58	31	40	0.31
	C-12	36.6	45	39	26	19	0.38
	C-21	54.0	71	57	31	40	0.31
	C-22	19.2	31	19	7	24	−0.02
	C-31	54.5	71	59	34	37	0.37
	C-32	37.5	51	40	21	30	0.28
2b	C-11	57.7	70	63	41	29	0.54
	C-12	36.1	53	38	17	35	0.20
	C-21	48.3	64	54	27	36	0.45
	C-22	21.2	42	21	1	41	−0.03
	C-31	54.3	68	55	41	27	0.06
	C-32	42.3	58	46	23	36	0.3

[a]Values of CST parameters for aromatic and carbonyl groups are reported in previously published work (refs 22 and 23). [b]Span is expressed as $\Omega = \delta_{11} - \delta_{33}$. [c]Skew is expressed as $\kappa = (\delta_{22} - \delta_{iso})/\Omega$.

(ii). ^{13}C 2D PASS Analysis of the CST Parameters for 1 and 2. Correlation of Experimental and Calculated Data. Chemical shift tensor (CST) parameters can be obtained from analysis of the static line shape of ^{13}C nuclei. Static CST principal component measurements can be only used with simple molecules or simple labeling schemes because of spectral overlap and also suffer from sensitivity issues in natural abundance systems, while 1D CP/MAS methods also suffer from similar limitations. This drives the need for 2D NMR techniques in the more complex molecules. 2D NMR methods

dx.doi.org/10.1021/jp2111567 | J. Phys. Chem. B 2012, 116, 1974−1983

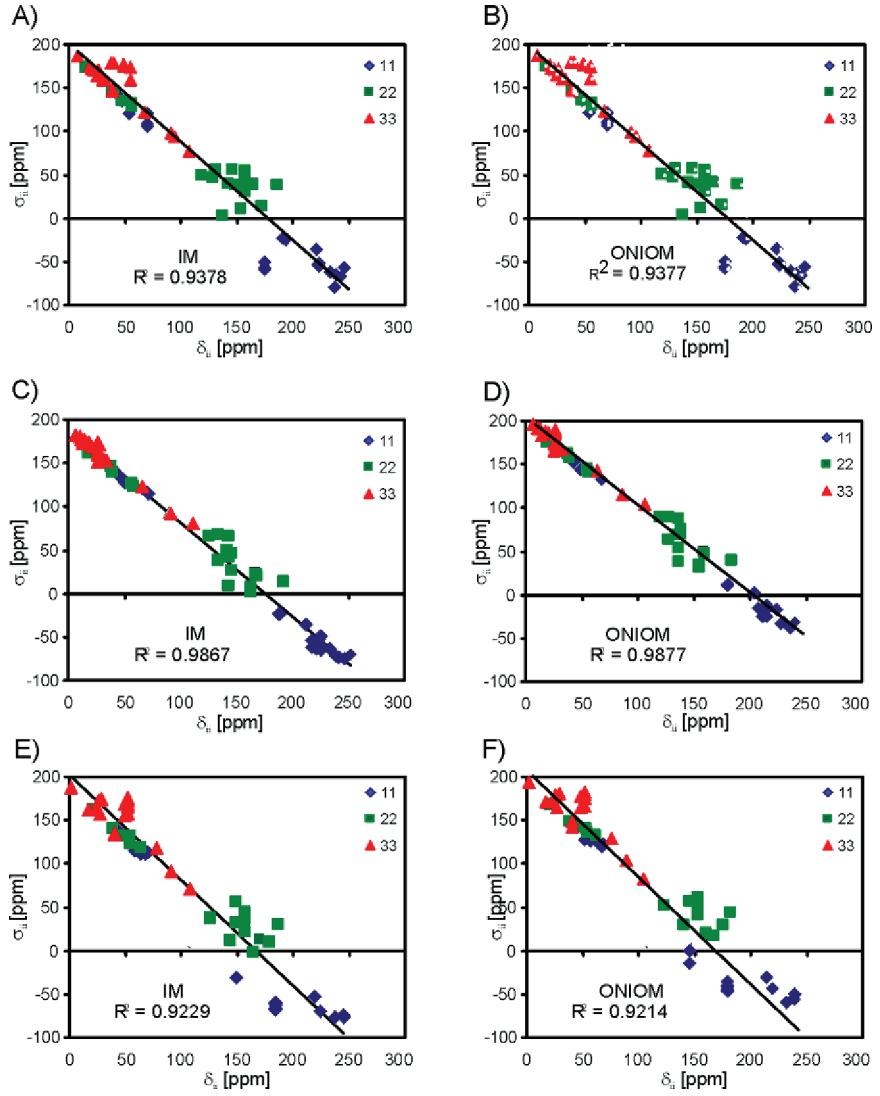

Figure 6. Correlation of experimental chemical shift tensor values (δ_{ii}) and calculated nuclear shielding parameters (σ_{ii}) of the YAF peptides using IM (A) **1**, (C) **2a**, and (E) **2b** as well as ONIOM (B) **1**, (D) **2a**, and (F) **2b**.

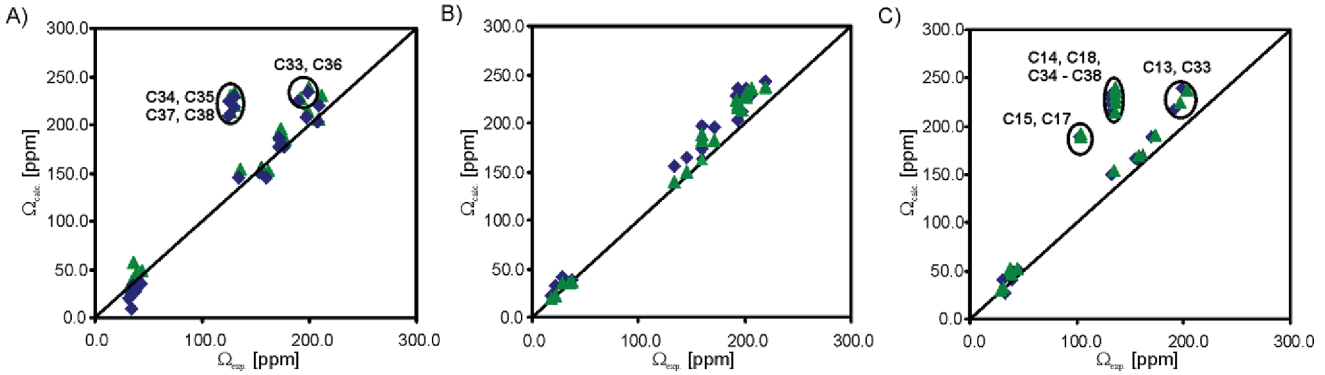

Figure 7. Correlation between the experimental span (Ω_{exp}) and calculated span values (Ω_{calc}) using DFT GIAO IM and ONIOM methodology for (A) sample **1**, (B) sample **2a**, and (C) sample **2b**. Blue diamonds represents IM data and the green triangles represent the ONIOM data. Solid lines indicate ideal correlation with a slope equal to 1.

can be employed to assign the values of the principal elements ^{13}C δ_{ii} (ii = 11, 22, and 33) of the chemical shift tensor (CST) that defines the line shape. There are several approaches that allow the separation of the isotropic and anisotropic portions of the spectra for heavily overlapped systems.[39−42] In this work, we employed the 2D PASS sequence for analysis of ^{13}C spectra.[43] This technique offers good sensitivity compared to other methods and does not require hardware modifications or a special probe head.

In our previous papers, we reported ^{13}C δ_{ii} parameters for the aromatic and carbonyl atoms of samples **1** and **2** analyzing 2D

dx.doi.org/10.1021/jp2111567 | J. Phys. Chem. B 2012, 116, 1974−1983

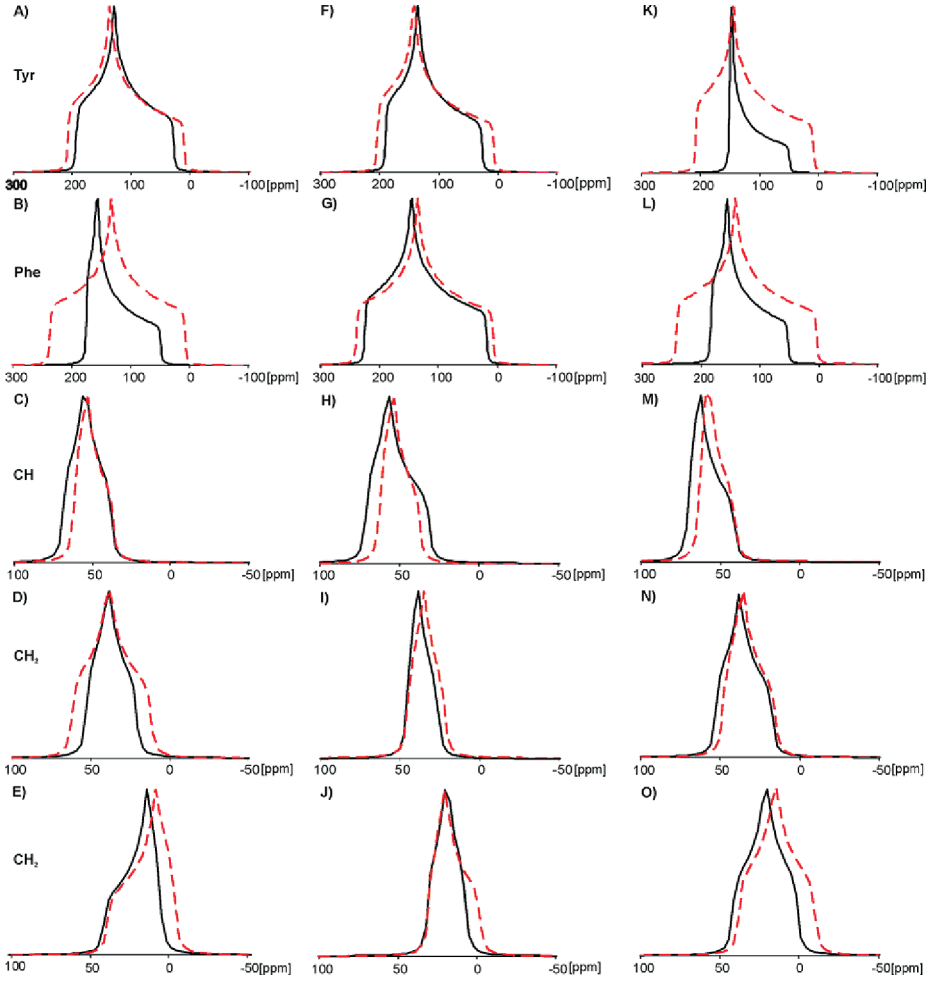

Figure 8. Correlation static experimental and computed CSA line shape for sample **1** (left column), **2a** (middle column), and **2b** (right column). Black solid line, experimental; red dashed line, theory.

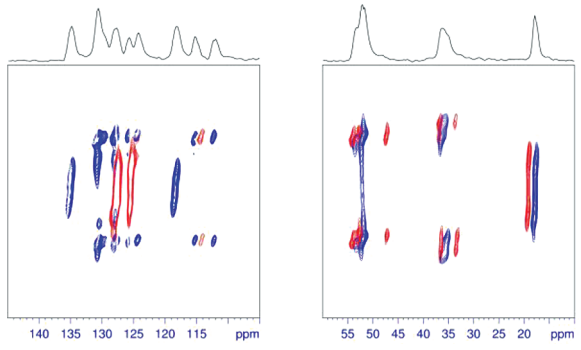

Figure 9. 2D PISEMA MAS overlapped spectra for sample **1** (red) and **2a** (blue) in the aromatic (left) and aliphatic regions (right). 1D projection represents sample **2a**.

PASS spectra recorded at 2 kHz spinning rate.[23,24] Because the anisotropy of aliphatic carbons is much lower compared to the aromatic and carbonyl carbons, the spinning rate must be in the range of 1.0−1.5 kHz to obtain sufficient number of spinning sidebands for simulation. Figure 5 displays the 2D PASS spectrum of **2a** measured with a sample rotation 1 kHz. A similar procedure was employed to study **1** and **2b**. The spectrum exhibits a complex pattern under slow sample spinning. Using proper data shearing (Figure 5B), it is possible to separate the spinning sidebands for each carbon and to use a calculational procedure to establish the ^{13}C δ_{ii} parameters.

It is clear from such a presentation that the F2 projection corresponds to the infinite spinning speed spectrum, whereas F1 represents CSA. For fitting of the spinning sideband pattern of the F1 spectra, we have employed a previously published protocol.[23,24] The values of the selected ^{13}C δ_{ii} parameters for **1** and **2** are presented in Table 1.

Figure 6 shows the correlation between the experimental and calculated shielding parameters obtained employing the DFT GIAO approach for the IMs and clusters (samples **1**, **2a**, and **2b**). In contrast to the plots shown in Figure 4, the correlation of the CST parameters was poor, especially for samples **1** and **2b**. The scattering of the experimental points is apparent, and the values of the R^2 parameters for both methods are lower compared to correlations of the isotropic values. For sample **2a** (Figure 6C and Figure 6D), a comparable analysis of the plots indicates a slightly better correlation for the cluster calculation. For ONIOM, the R^2 is equal to 0.9877, whereas for IM, it is equal to 0.9867. It is interesting to note that this sample cluster molecule correlates well in the region of the δ_{22} parameters, which are very sensitive to intermolecular contacts (e.g., hydrogen bonding with contribution of C═O peptide groups).[44]

The plot of the experimental and calculated span values ($\Omega = \delta_{11} - \delta_{33}$) for all of the studied samples is displayed in Figure 7.

dx.doi.org/10.1021/jp2111567 | J. Phys. Chem. B 2012, 116, 1974−1983

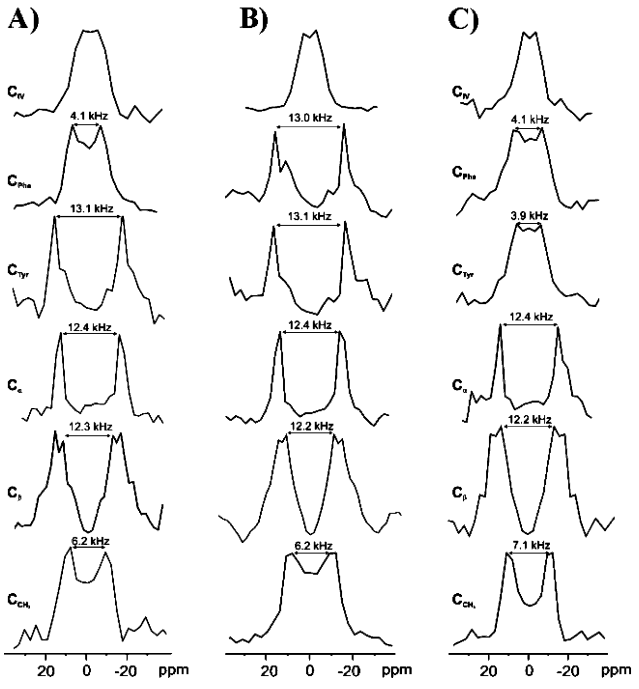

Figure 10. Projection along F1 for selected carbon atoms of (A) **1**, (B) **2a**, and (C) **2b** with labeled splitting between the singularities of doublets.

Scheme 2. Selectively ^{2}H Labeled YAF Models Used in Our Project (A) Tyr-d_4-Ala-Phe and (B) Tyr-Ala-Phe-d_5

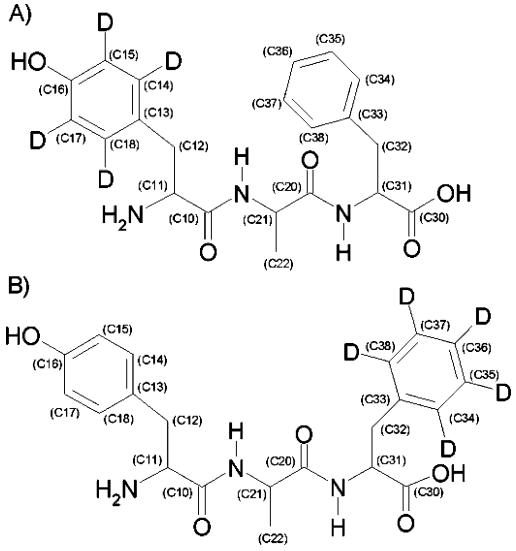

For an ideal correlation, the slope is equal to 1 (represented by solid line in figures). For samples **1** and **2b**, both DFT GIAO calculations (IM, ONIOM) provide a similar set of data. It is apparent that the experimental span values for the phenyl ring of **1** represented by C34, C35 and C37, C38 as well C33, C36 carbons do not fit the calculated data (Figure 7A). The correlation for **2a** (Figure 7B) is much better, and the scattering of the experimental data points is not considerable. In contrast, the distribution of the experimental points, for sample **2b** shown in Figure 7C, is significant. The most spread out points represent aromatic rings of the phenylalanine and tyrosine. It has to be stressed that, for the other carbons in the side groups and main skeleton, the correlation of Ω_{exp} and Ω_{calc} is relatively good.

To visualize the supra effect, we compared the static ^{13}C line shapes sketched with the δ_{ii} parameters obtained from the 2D PASS experiment with the line shapes drawn using the calculated σ_{ii} shielding parameters obtained from the ONIOM method (Figure 8).

The left, middle, and right column of Figure 8 represent YAF **1**, **2a**, and **2b**, respectively. The solid black lines represent the experimental spectra, and the red broken lines display the calculated spectra. It is apparent from analysis of the static line shapes that, for sample **1**, the correlation for the tyrosine ring is good, whereas for the phenylalanine ring, the calculated line shape is dramatically different compared to the experimental spectrum (Figure 8B). For the other aliphatic signals, the correlation between the experimental and calculated spectra is acceptable even though the calculated σ_{ii} values appear to be underestimated for the CH carbons. For sample **2a** (middle column), there is good correlation between the experimental and calculated line shapes, both in aromatic and aliphatic regions. In contrast, for sample **2b** (right column), only the aliphatic carbons correlate well, while there is no correlation for the aromatic groups (i.e., tyrosine (Figure 8K) and phenylalanine (Figure 8L) rings).

Our study clearly proves that the lack of correlation in some cases does not indicate weakness of the theoretical approach but is related to the nature of the systems under investigation. The discrepancy between the experimental and calculated ^{13}C CST parameters for selected groups of carbon signals suggests that there is a variation in the flexibility of the side chains and rigid backbone of the studied peptides. This problem is discussed in detail in the following sections.

(iii). PISEMA MAS Study of the Molecular Dynamics. The preliminary results regarding the distinct dynamics of the YAF peptides were obtained using dipolar recoupling experiments, which are well suited for simultaneously measuring motional averaging at multiple sites in biomolecules.[45−47] In the two-dimensional (2D) experiments, the separated local field sequences can reintroduce dipolar anisotropic interactions and correlate them to the isotropic chemical shifts.[48] The Lee−Goldburg cross-polarization (LGCP)[49−51] and polarization inversion spin exchange at the magic angle (PISEMA)[52] pulse sequences were recently used to correlate the motional average anisotropic dipolar interactions with high-resolution chemical shift dimensions during MAS in the 2D approach. For analysis of the effect of molecular motion on the line shape of the dipolar spectra, we have employed a modified sequence of PISEMA MAS as reported by Dvinskikh et al.[20]

Figure 9 shows the 2D PISEMA MAS spectra for sample **1** and **2a** recorded with a spinning rate of 13 kHz at ambient temperature. The ^{1}H effective field strength, ω_{1Heff}, was held constant, while the ^{13}C spin-lock field strength was matched using $\omega_{1Heff} \pm \omega_{13C} = n\omega_r$ (n = 1, −1). The SEMA contact time was incremented asynchronously with rotation to yield the heteronuclear dipolar dimension of the 2D experiment. The ^{13}C spin isotropic chemical shift was detected in the second dimension of the experiment.

Figure 10 shows the F1 slices for the selected carbon atoms of **1** and **2** with labeled splitting between the singularities of the doublets. These doublets reflect the dipolar coupling between the proton and carbon. For ^{13}C−^{1}H, the r_{ij} distance was equal to 1.09 Å, δ the dipolar coupling constant for the rigid-limit is

dx.doi.org/10.1021/jp2111567 | J. Phys. Chem. B 2012, 116, 1974−1983

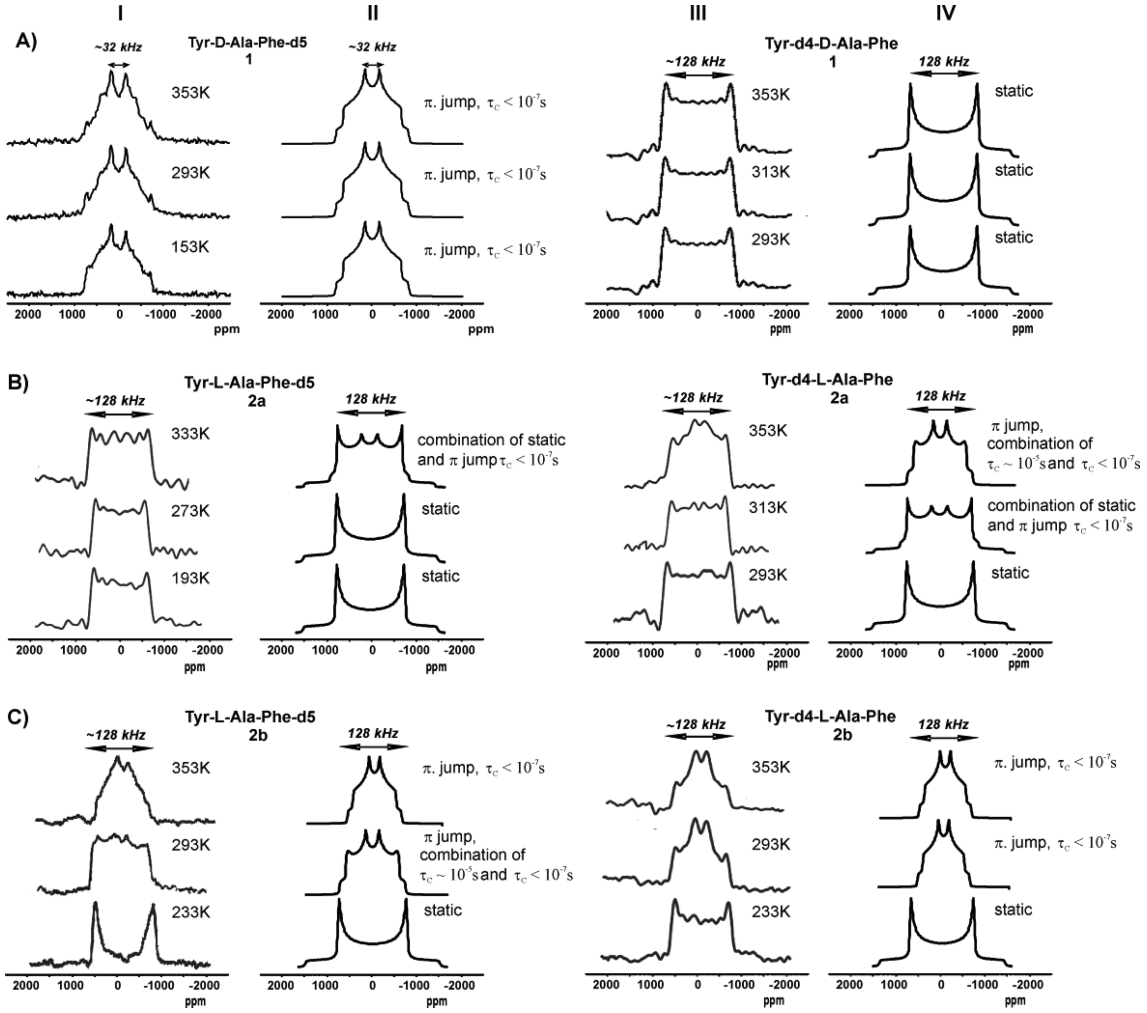

Figure 11. Experimental (column I and III) and simulated (column II and IV) ^{2}H spectra for samples **1**, **2a**, and **2b**. The spectra were simulated using the EXPRESS 1.0[62] application performed in the MATLAB R2010b environment and the NMR-WEBLAB V4.3.2 software.[63] The line shape was apodized by Lorentzian function with line broadening equal to 2 kHz.

22.7 kHz according to the following equation:

$$\delta = -\frac{\mu_0 \hbar^2}{4\pi} \frac{\gamma_i \gamma_j}{r_{ij}^3}$$

The experimental values of the splitting shown in Figure 10 are smaller compared to the calculated coupling, because δ is reduced by a scaling factor (sf). As previously demonstrated, the dipolar sf in the PISEMA experiment is very sensitive to the amplitudes of the two RF spin-lock fields as well as the mismatch parameter $\Delta = \omega_{\text{eff}} - \omega_{1S}$. The discrepancy between the predicted and measured δ values was exhaustively discussed by Fu et al.[53] For the PISEMA MAS, the exact Hartmann−Hahn matching condition yields a maximum scaling factor of 0.584 (cos 54.7°). In the case of a mismatch, the scaling factor can be much lower. For the rigid system, the expected value of δ is ca. 13.0 kHz (22.7 kHz × 0.584). Fast molecular motion can reduce the principal component of the dipolar tensor by a factor (S), which is known as the order parameter. S ranges from 0.5 to 1. The latter value represents a rigid system.

The order parameters related to the dynamic models, including diffusion in a cone and the three-site hop for aliphatic groups as well two-site jumping or diffusion in a flattened cone that is typical for dynamics of phenyl rings, have been reported.[51,54] Inspection of the splitting values shown in Figure 10 clearly indicate distinct molecular motion of aromatic groups. For sample **1**, the tyrosine ring is rigid, while the phenylalanine ring undergoes fast molecular motion (splitting equal to 13.1 and 4.1 kHz). For YAF **2a**, both aromatic rings are rigid, while for **2b**, both rings are mobile (splitting equal to 4.1 kHz). In addition, the values for the aliphatic carbons are comparable, which shows that the main skeleton of peptides is rather rigid. The methyl groups for all three samples are undergoing fast molecular motion even though they exhibit slightly different splitting equal to 6.2 (**1**), 6.2 (**2a**), and 7.1 kHz (**2b**).

(iv). ^{2}H NMR Study of the Molecular Motion of the Phenyl Rings for Selectively Labeled 1 and 2 YAF. In this section, we report further study of the motion of the phenylalanine and tyrosine rings in the crystal lattice utilizing solid-state ^{2}H NMR spectroscopy. Selectively ^{2}H labeled YAF models used in our study are shown in Scheme 2. Solid-state ^{2}H NMR spectroscopy of the deuterium-labeled samples provided detailed information on the molecular motion in the frequency range of 10^3 to 10^6 Hz as well as the characteristics of the motion, such as free rotation or a 180° flipping motion of the phenyl ring about a symmetry axis.[55]

The molecular motion of the phenyl rings of the Phe residues in the solids has been extensively studied by ^{2}H NMR

dx.doi.org/10.1021/jp2111567 | J. Phys. Chem. B 2012, 116, 1974−1983

spectroscopy for amino acids, polypeptides, and proteins.[56−59] Hiraoki and co-workers exploring the phenyl ring dynamics of poly(L-phenylalanine) as a function of temperature and echo delay time have revealed that the π-flipping motion is characterized by a fairly broad distribution of correlation times and strongly dependent on the temperature.[60] Kamihira et al. have reported detailed analysis of the molecular dynamics of enkephalin, one of the best-characterized opioid peptides.[61] These observations suggest that the degree of motion in the aromatic rings of the phenylalanine and tyrosine residues strongly depends on the environment of the enkephalin molecules, such as the crystalline packing and the state of the bound solvents.

Figure 11 shows the static ^{2}H NMR spectra for sample **1** (upper row, Figure 11A), **2a** (middle row, Figure 11B) and **2b** (bottom row, Figure 11C) recorded using a quadrupolar echo pulse sequence with temperatures, as indicated in Figure 11. The experimental spectra for the samples with the deuterium labeled phenylalanine ring are shown in column I, while the experimental spectra for the samples with the labeled tyrosine ring are shown in column III. Column II and IV show the simulated spectra with the established values of the correlation times (τ_c) and geometry of the molecular motion. For fitting experimental line shapes for peptides **2a** and **2b,** a combination of two subspectra with different correlation times (τ_c) was employed.

We assumed that, in the unit cell containing a number of molecules, some of them could undergo dynamic processes on different time scales. Such phenomenon was experimentally illustrated by Torchia and co-workers,[64] who analyzed the deuterium spectra of methionine to reveal different molecular motions for the two molecules in the asymmetric unit of the crystal lattice.

It is important to note that ^{2}H results are in excellent agreement with the PISEMA experiments performed at ambient temperature. Variable temperature ^{2}H measurements prove that the tyrosine and phenylalanine rings in samples **2a** and **2b** became more mobile with increasing temperature. In contrast, the aromatic rings of sample **1** preserve their dynamics regime (static tyrosine and π-jumping phenylalanine) in a large range of temperatures.

CONCLUSIONS

The X-ray coordinates are often used for structure assignment of the chemical shift parameters by employing theoretical methods. With recent progress in QM methodology, the correlations between experimental data and theoretical calculations are generally excellent, which is due to the fact that modern algorithms take into consideration a number of structural parameters (e.g., intra- and intermolecular interactions, $\pi-\pi$ stacking, lattice periodicity, etc.), which has an influence on the quality of the computed results. Therefore, in the light of recent achievements, there is no surprise that the theoretical data, which did not perfectly fit the experimental results, might be a source of frustration for researchers. In our work we show that in some cases scattering of data should be no matter of worries but rather considered as a source of important structural information.

In this project, we have tested DFT methodology for isolated molecules (IMs) and clusters employing rigid and flexible peptide models with large-scale amplitude motions in the crystal lattice. For a rigid system, ONIOM is slightly better than IM in its ability to reproduce experimental chemical shift parameters, especially for those centers that contributed to intra- and/or intermolecular contacts. Both methods are not able to reproduce the shielding parameters for systems under a dynamic regime.

Finally, we wish to highlight the attractiveness of YAF peptides as testing samples for development of solid-state NMR methodologies and, in particular, for those sequences that are sensitive to large scale molecular dynamics in the solid state as well as challenging samples for theoretical calculation of NMR shielding.

ASSOCIATED CONTENT

Supporting Information

Visualizations of cluster (CM calculations) for structures **1**, **2a**, and, **2b** (Figures S1−S3). Tables of NMR data for strustures **1**, **2a**, and **2b** (Tables S1−S9). This material is available free of charge via the Internet at http://pubs.acs.org.

AUTHOR INFORMATION

Corresponding Author

*E-mail: marekpot@cbmm.lodz.pl.

Notes

The authors declare no competing financial interest.

ACKNOWLEDGMENTS

The authors are grateful to the State Committee for Scientific Research (MIiN) for financial support, Grant No. N N204 131335. This work was partially supported by the Ministry of Education, Youths and Sports of the Czech Republic (MSMT 2B08021). The computational resources were partially provided by the Polish Infrastructure for Supporting Computational Science in the European Research Space (PL-GRID) and under the program "Projects of Large Infrastructure for Research, Development, and Innovations" LM2010005.

REFERENCES

(1) Abragam, A. *The Principles of Nuclear Magnetism*; Claderon Press: Oxford, U.K., 1994.

(2) (a) Levitt, M. H. *Spin Dynamics: Basics of Nuclear Magnetic Resonance*; Wiley: New York, 2007, (b) Jacobsen, N. E. Simplified Theory. *Applications and Examples for Organic Chemistry and Structural Biology*; Wiley: New York, 2007.

(3) Friebolin, H. *Basic One- and Two-Dimensional NMR Spectroscopy*; Wiley VCH Verlag GmbH: Weinheim, Germany, 2004.

(4) Jackowski, K. *J. Mol. Struct.* **2006**, *786*, 215−219.

(5) Casabianca, L. B.; Dios, D.; Angel, C. *J. Chem. Phys.* **2008**, *128*, 052201and references cited therein.

(6) Grant, D. M.; Facelli, J. C.; Alderman, D. W.; Sherwood, M. H.; Tossell, J. A. *Nuclear Magnetic Shielding and Molecular Structure*; Kluwer Academic Publishers: Dordrecht, The Netherlands, 1993; p 367.

(7) Malkin, V. G.; Malkina, O. L.; Eriksson, L. A.; Salahub, D. R.; Seminaro, J. M.; Politzer, P. Modern density functional theory: a tool for chemistry. *Theoretical and Computational Chemistry*; Elsevier: Amsterdam, 1995; Vol. 2.

(8) (a) Facelli, J. C. *Prog. Nucl. Magn. Reson. Spectrosc.* **2011**, *58*, 176−201. (b) Saito, H.; Ando, I.; Ramamoorthy, A. *Prog. Nucl. Magn. Reson. Spectrosc.* **2010**, *57*, 181−228 and references cited therein.

(9) Orendt, A. M.; Facelli, J. C. *Annu. Rep. NMR Spectrosc.* **2007**, *62*, 115−178.

(10) Robinson, M.; Haynes, P. D. *J. Chem. Phys.* **2010**, *133*, 084109.

(11) Dumez, J. N.; Pickard, C. J. *J. Chem. Phys.* **2009**, *130*, 104701.

(12) De Gortari, I.; Portella, G.; Salvatella, X.; Bajaj, V. S.; van der Wel, P. C.; A, Yates, J. R.; Segall, M. D.; Pickard, C. J.; Payne, M. C.; Vendruscolo, M. *J. Am. Chem. Soc.* **2010**, *132*, 5993−6000.

(13) Carignani, E.; Borsacchi, S.; Marini, A.; Mennucci, B.; Geppi, M. *J. Phys. Chem. C* **2011**, *115*, 25023−25029.
(14) Erspamer, V *Int. J. Dev. Neurosci.* **1992**, *10*, 3−30.
(15) Jilek, A.; Kreil, G. *Monatsh. Chem.* **2008**, *139*, 1−5.
(16) Morcombe, C. R.; Zilm, K. W. *J. Magn. Reson.* **2003**, *162*, 479−486.
(17) Metz, G.; Wu, X.; Smith, S. O. *J. Magn. Reson. Ser. A* **1994**, *110*, 219−227.
(18) Bennett, A. W.; Rienstra, C. M.; Auger, M.; Lakshmi, K. V.; Griffin, R. G. *J. Chem. Phys.* **1995**, *103*, 6951.
(19) Topspin, Version 2.1; Germany.
(20) Dvinskikh, S. V.; Sandstrom, D. *J. Magn. Reson.* **2005**, *175*, 163−169.
(21) Antzutkin, O. N.; Shekar, S. C.; Levitt, M. H. *J. Magn. Reson., Ser. A* **1995**, *115*, 7−19.
(22) Frisch, M. J.; Trucks, G. W.; Schlegel, H. B.; Scuseria, G. E.; Robb, M. A.; Cheeseman, J. R.; Scalmani, G.; Barone, V.; Mennucci, B.; Petersson, G. A.; Nakatsuji, H.; Caricato, M.; Li, X.; Hratchian, H. P.; Izmaylov, A. F.; Bloino, J.; Zheng, G.; Sonnenberg, J. L.; Hada, M.; Ehara, M.; Toyota, K.; Fukuda, R.; Hasegawa, J.; Ishida, M.; Nakajima, T.; Honda, Y.; Kitao, O.; Nakai, H.; Vreven, T.; Montgomery, J. A.; , Jr., Peralta, J. E.; Ogliaro, F.; Bearpark, M.; Heyd, J. J.; Brothers, E.; Kudin, K. N.; Staroverov, V. N.; Kobayashi, R.; Normand, J.; Raghavachari, K.; Rendell, A.; Burant, J. C.; Iyengar, S. S.; Tomasi, J.; Cossi, M.; Rega, N.; Millam, J. M.; Klene, M.; Knox, J. E.; Cross, J. B.; Bakken, V.; Adamo, C.; Jaramillo, J.; Gomperts, R.; Stratmann, R. E.; Yazyev, O.; Austin, A. J.; Cammi, R.; Pomelli, C.; Ochterski, J. W.; Martin, R. L.; Morokuma, K.; Zakrzewski, V. G.; Voth, G. A.; Salvador, P.; Dannenberg, J. J.; Dapprich, S.; Daniels, A. D.; Farkas, O.; Foresman, J. B.; Ortiz, J. V.; Cioslowski, J.; , Fox, D. J. *Gaussian 09*, revision A.02; Gaussian, Inc.: Wallingford, CT, 2009.
(23) Słabicki, M. M.; Potrzebowski, M. J.; Bujacz, G.; Olejniczak, S.; Olczak, J. *J. Phys. Chem. B* **2004**, *108*, 4535−4545.
(24) Trzeciak-Karlikowska, K.; Bujacz, A.; Jeziorna, A.; Ciesielski, W.; Bujacz, G. D.; Gajda, J.; Pentak, D.; Potrzebowski, M. *J. Cryst. Growth Des.* **2009**, *9*, 4051−4059.
(25) Becke, A. D. *J. Chem. Phys.* **1993**, *98*, 5648−5652.
(26) Stephen, P. J.; Devlin, F. J.; Chabalowski, C. F.; Frisch, M. J. *J. Phys. Chem.* **1994**, *98*, 11623.
(27) Hariharan, P. C.; Pople, J. A. *Theoret. Chimica Acta* **1973**, *28*, 213−222.
(28) Francl, M. M.; Petro, W. J.; Hehre, W. J.; Binkley, J. S.; Gordon, M. S.; DeFrees, D. J.; Pople, J. A. *J. Chem. Phys.* **1982**, *77*, 3654−3665.
(29) Krishnan, R.; Binkley, J. S.; Seeger, R.; Pople, J. A. *J. Chem. Phys.* **1980**, *72*, 650−654.
(30) Helgaker, T.; Jørgensen, P. *J. Chem. Phys.* **1991**, *95*, 2595−2601.
(31) Grimme, S. *J. Comput. Chem.* **2004**, *25*, 1463−1473.
(32) Ernzerhof, M.; Scuseria, G. *J. Chem. Phys.* **1999**, *110*, 5029−5036.
(33) Maseras, F.; Mokomura, K. *J. Comput. Chem.* **1995**, *16*, 1170−1179.
(34) Rappe, A. K.; Casewit, C. J.; Colwell, K. S.; Goddard, W. A.; Skiff, W. M. *J. Am. Chem. Soc.* **1992**, *114*, 10024−10035.
(35) Van Wuellen, C. *Phys. Chem. Chem. Phys.* **2000**, *2*, 2137−2144.
(36) (a) Sebastiani, D. *Mod. Phys. Lett. B* **2003**, *17*, 1301. (b) Widdifield, C. M.; Schurko, R. W. *Concepts Magn. Reson. Part A* **2009**, *34A*, 91. (c) Weber, J.; Gunne, J. S. A. D. *Phys. Chem. Chem. Phys.* **2010**, *12*, 583−603.
(37) Liu, W.; Wang, W. D.; Wang, W.; Bai, S.; Dybowski, C. *J. Phys. Chem. B* **2010**, *114*, 16641−16649.
(38) Nowicka, K.; Bujacz, A.; Paluch, P.; Sobczuk, A.; Jeziorna, A.; Ciesielski, W.; Bujacz, G. D.; Jurczak, J.; Potrzebowski, M. J. *PhysChemChemPhys* **2011**, *13*, 6423−6433.
(39) Hu, J.; Wang, W.; Liu, F.; Solum, M. S.; Alderman, D. W.; Pugmire, R. J. *J. Magn. Reson., Ser. A* **1995**, *113*, 210−222.
(40) Alderman, D. W.; McGeorge, G.; Hu, J. Z.; Pugmire, R. J.; Grant, D. M. *Mol. Phys.* **1998**, *95*, 1113−1126.
(41) Frydman, L.; Chingas, G. C.; Lee, Y. K.; Grandinetti, P. J.; Eastman, M. A.; Barral, G. A.; Pines, A. *J. Chem. Phys.* **1992**, *97*, 4800−4808.
(42) Kolbert, A. C.; Griffin, R. G. *Chem. Phys. Lett.* **1990**, *166*, 87−91.
(43) Antzutkin, O. N.; Shekar, S. C.; Levitt, M. H. *J. Magn. Reson. Ser. A* **1995**, *115*, 7−19.
(44) (a) Wei, Y.; Lee, D. K.; Ramamoorthy, A. *J. Am. Chem. Soc.* **2001**, *123*, 6118−6126. (b) Birn, J.; Poon, A.; Mao, Y.; Ramamoorthy, A. *J. Am. Chem. Soc.* **2006**, *126*, 8529−8534.
(45) Ladizhansky, V. *Solid State Nucl. Mag.* **2009**, *36*, 119−128.
(46) Wylie, B. J.; Rienstra, C. M. *J. Chem. Phys.* **2008**, *128*, 052207.
(47) Drobny, G. P.; Long, J. R.; Karlsson, T.; Shaw, W.; Popham, J.; Oyler, N.; Bower, P.; Stringer, J.; Cregory, D.; Mehta, M. A.; Stayton, P. S. *Annu. Rev. Phys. Chem.* **2003**, *54*, 531−571.
(48) Schmidt-Rohr, K.; Spiess, H. W. *Multidimensional Solid-State NMR And Polymers*; Academic Press: London, 1994.
(49) Cobo, M. F.; Malinakova, K.; Reichert, D.; Saalwachter, K.; Deazevedo, E. R. *Phys. Chem. Chem. Phys.* **2009**, *11*, 7036−7047.
(50) Ladizhansky, V.; Vega, S. *J. Chem. Phys.* **2000**, *112*, 7158−7167.
(51) Hong, M.; Yao, X.; Jakes, K.; Huster, D. *J. Phys. Chem. B* **2002**, *106*, 7355−7364.
(52) Ramamoorthy, A.; Wei, Y.; Lee, D. K. *Annu. Rep. NMR Spectrosc.* **2004**, *52*, 1−52.
(53) Fu, R.; Tian, C.; Kim, H.; Smith, S. A.; Cross, T. A. *J. Magn. Reson.* **2002**, *159*, 167−174.
(54) Lorieau, L. J.; Day, L. A.; McDermott, A. E. *Magn. Reson. Chem.* **2006**, *44*, 334−347.
(55) Spiess, H. W. C. *Polym. Sci.* **1983**, *261*, 193−209.
(56) Gall, C. M.; Diverdi, J. A.; Opella, S. J. *J. Am. Chem. Soc.* **1981**, *103*, 5039−5043.
(57) Schaefer, J.; Stejskal, E. O.; McKay, R. A. *J. Magn. Reson.* **1984**, *57*, 85−90.
(58) Frey, M. H.; DiVerdi, J. A.; Opella, S. J. *J. Am. Chem. Soc.* **1985**, *107*, 7311−7315.
(59) Hiyama, Y.; Silverton, J. V.; Torchia, D. A.; Gerig, J. T.; Hammond, S. J. *J. Am. Chem. Soc.* **1986**, *108*, 2715−2723.
(60) Hiraoki, T.; Kogame, A.; Nishi, N.; Tsutsumi, A. *J. Mol. Struct.* **1998**, *441*, 243−250.
(61) Kamihira, M.; Naito, A.; Tuzi, S.; Saito, H. *J. Phys. Chem. A* **1999**, *103*, 3356−3363.
(62) Vold, R. L.; Hoaston, G. L. *J. Magn. Reson.* **2009**, *198*, 57−72.
(63) Macho, V.; Brombacher, L.; Spiess, H. W. *Appl. Magn. Reson.* **2001**, *20*, 405−432.
(64) Sparks, S. W.; Budhu, N.; Young, P. E.; Torchia, D. A. *J. Am. Chem. Soc.* **1988**, *110*, 3359−3367.